Structural Monitoring and Maintenance, *Vol. 9, No. 3 (2022) 237-258*
https://doi.org/10.12989/smm.2022.9.3.237

A baseline free method for locating imperfect bolted joints

Reza Soleimanpour*[1], Sayed Mohamad Soleimani [1a]
and Mariam Naser Sulaiman Salem [1b]

College of Engineering, Department of Civil Engineering, Australian University, Kuwait

(*Received February 15, 2022, Revised July 16, 2022, Accepted July 30, 2022*)

Abstract. This paper studies detecting and locating loose bolts using nonlinear guided waves. The 3D Finite Element (FE) simulation is used for the prediction of guided waves' interactions with loose bolted joints. The numerical results are verified by experimentally obtained data. The study considers bolted joints consisting of two bolts. It is shown that the guided waves' interaction with surfaces of a loose bolted joint generates Contact Acoustic Nonlinearity (CAN). The study uses CAN for detecting and locating loose bolts. The processed experimentally obtained data show that the CAN is able to successfully detect and locate loose bolted joints. A 3D FE simulation scheme is developed and validated by experimentally obtained data. It is shown that FE can predict the propagation of guided waves in loose bolts and is also able to detect and locate them. Several numerical case studies with various bolt sizes are created and studied using the validated 3D FE simulation approach. It is shown that the FE simulation modeling approach and the signal processing scheme used in the current study are able to detect and locate the loose bolts in imperfect bolted joints. The outcomes of this research can provide better insights into understanding the interaction of guided waves with loose bolts. The results can also enhance the maintenance and repair of imperfect joints using the nonlinear guided waves technique.

Keywords: 3D finite element; anti-asymmetric guided waves; contact acoustic nonlinearity; damage detection; damage localization; imperfect bolted joints

1. Introduction

The importance of bolted connection in various structures such as buildings, bridges, aircraft, and pipelines is paramount. Bolted connections are reliable, cost-effective, easy to install, and widely used due to their high bearing capacity. However, the global structural behavior is greatly influenced by the quality of the bolted joints. The development of a small flaw in the bolted joint may be catastrophic as it can lead to connection failure and may severely impact structural reliability and safety. That is why engineers pay special attention to the quality of bolted joints during the design, assembly, and construction stages. However, bolted joint failures still happen due to design or assembly errors. Therefore, it is important to detect and fix those flaws at their early stages to avoid serious damage to the structure. Detecting and locating incipient defects enables defect monitoring during the service life of a structure and provides the opportunity for

*Corresponding author, Assistant Professor, E-mail: r.soleimanpour@ack.edu.kw
[a] Associate Professor, E-mail: smsoleimani@yahoo.com
[b] Research Assistant, E-mail: 1719394@ack.edu.kw

 ISSN: 2288-6605 (Print), 2288-6613 (Online)

decision-making and setting preventative measures to avoid structural failure.

Bolted joints can fail due to several reasons such as crack, fatigue, excessive load, and looseness. Loosen bolts in a structure will severely impact its capacity and may have severe consequences such as global failure in the structure or fluid leakage and interruption of service in the pipelines. Detecting loose bolted connections at an early stage can prevent failure of the structure. Looseness is usually initiated by slipping of bolted joint components due to vibration or external forces. Slippage of the connected plates leads to their vibration which in turn loosens the bolted joint.

1.1 Bolt loosening detection methods

Bolt loosening monitoring and identification have been subjects of interest for many years. A wide range of in situ visual inspection and sensor-based techniques have been developed for detecting bolt loosening. Several comprehensive studies in these fields focused on detecting imperfect joints. The bolt loosening detections are commonly divided into direct and indirect measurement methods. Direct tension indicator, strain gauge, and control torque methods are among common direct measurement methods. Although these techniques are commonly used in practice, however, they do not allow for online monitoring of the bolted joint and their accuracy and reliability can be affected by human errors and may not be up to a satisfactory level. Impedance method, vibration-based method, conventional ultrasonic method, acoustoelastic method, and guided waves are some examples of indirect inspection techniques for bolt loosening. Unlike direct methods, indirect methods allow for online monitoring of the bolts and usually have an acceptable level of accuracy and reliability for monitoring the bolted joints. However, the majority of these techniques rely on baseline data for detecting the loose bolted joints and are limited to the damage detection level only. The study on indirect methods is moving at a high pace. Recently, Wang *et al*. (2019) delivered a percussion-based method using analytical modeling and numerical simulation approaches verified by experiment for bolt loosening detection which did not require sensors attachment and considered the effect of bolted interfacial roughness. It was shown that the proposed method can successfully detect loose bolts. The aforementioned study was further developed for multi-bolt loosening detection in a recent study (Wang and Song 2020).

1.2 Guided waves technique applications

Among the developed techniques, the guided waves technique has attracted the attention of researchers due to its favorable benefits over the other non-destructive techniques (NDTs) such as improved reliability, long-range inspection, cost-effectiveness, and sensitivity to micro-scale defects. The guided waves technique has shown successful applications in bars, cables, beams, plates, and pipes. This technique also has a strong potential for detecting and locating damage of various kinds such as holes, cracks, fatigue, impact, and delamination for both isotropic and anisotropic materials (Soleimanpour and Ng 2017, Fromme and Sayir 2002, Wang *et al*. 2009).

In the literature, the guided waves techniques are categorized based on the linear and nonlinear wave parameters used. The linear wave parameters are the wave attenuation, wave amplitude, and wave velocity while the nonlinear wave parameters include higher harmonics and side harmonics. The first technique is referred to as the linear guided waves technique whereas the latter is known as the nonlinear guided waves technique.

The term nonlinear indicates that the system's response frequency is different from the incident

wave frequency. The linear guided waves techniques typically require baseline data which may not be always available or if available, could be affected by the temperature or other environmental factors. This is considered one of the major drawbacks of the linear guide waves techniques. To address such issues, the researchers have tried to develop baseline-free techniques. Unlike the linear techniques, nonlinear guided waves techniques usually do not use baseline data because the techniques rely on the nonlinear guided waves' parameters which are more sensitive to micro-scale damages, and thus, they are more robust than the linear waves techniques for damage detection (Solodov *et al*. 2002). However, since nonlinear guided waves' parameters are sophisticated, the acquisition, measurement, and processing of those parameters involve more challenges. The nonlinear guided waves technique is a promising technique that has shown strong potential for the non-destructive evaluation of structures. This technique can detect micro-scale defects at their early stages, and therefore, is a cost-effective approach.

In recent years, due to the reliability and the favorable benefits that the nonlinear guided waves technique offers, the research into using this technique for the non-destructive evaluation of structures has been moving at a high pace. However, the development of a nonlinear guided waves inspection and evaluation scheme is usually a difficult task due to the complex nature of the guided waves.

The literature divides the sources of wave nonlinearity into material nonlinearity and Contact Acoustic Nonlinearity (CAN). There have been several works on wave nonlinearity due to material nonlinearity referred to as classical nonlinearity (Pruell *et al*. 2007, Kumar *et al*. 2009). However, the number of works on guided waves nonlinearity due to CAN referred to as non-classical nonlinearity is limited (Soleimanpour and Ng 2017, Solodov *et al*. 2002). For the first case, some of the incident wave frequency components are eliminated by material nonlinearity which works as a filter. This will generate other wave frequency components different from the incident wave frequency such as sub-harmonics or higher harmonics. However, for the second case, the clapping mechanism due to contact discontinuity caused by the incident wave generates the CAN. Similar to material nonlinearity, the CAN works as a filter. The defect surface works as a frequency filter which eliminates the fundamental wave frequency but allows the converted frequencies wave to pass.

In the literature, a limited number of research projects have studied CAN generation in breathing damages such as debonding, cracks, and delamination. A model was developed by Soldove *et al*. (2002) to explain the clapping mechanism and CAN generation in breathing cracks. A material with variable stiffness was used to model the breathing defect's behavior at different stages of the crack opening and closure. In this model, the compressional stress stiffness is zero when the crack fully opens which leads to the wave modification and thus generation of CAN. Richardson (1979) developed equations to describe the CAN generation in a model consisting of two semi-infinite elastic plates with planar interfaces. Nitesh *et al*. developed a scheme for detecting damages in composite laminates using nonlinear Lamb waves (Yelve *et al*. 2017). Soleimanpour *et al*. (2017) investigated the CAN generation in composite beams with delamination using numerical and experimental approaches.

It was shown that the nonlinear wave parameters can be used for detecting and locating delamination in composite beams. Moreover, an equation was formulated for locating delamination in composite beams. In other studies, the scattering of linear and nonlinear guided waves around defects in isotropic and anisotropic materials was investigated (Soleimanpour and Ng 2021, Soleimanpour and Soleimani 2022). The results show that the scattering of nonlinear guided waves, unlike the linear waves, in isotropic and anisotropic plates is complex and hard to

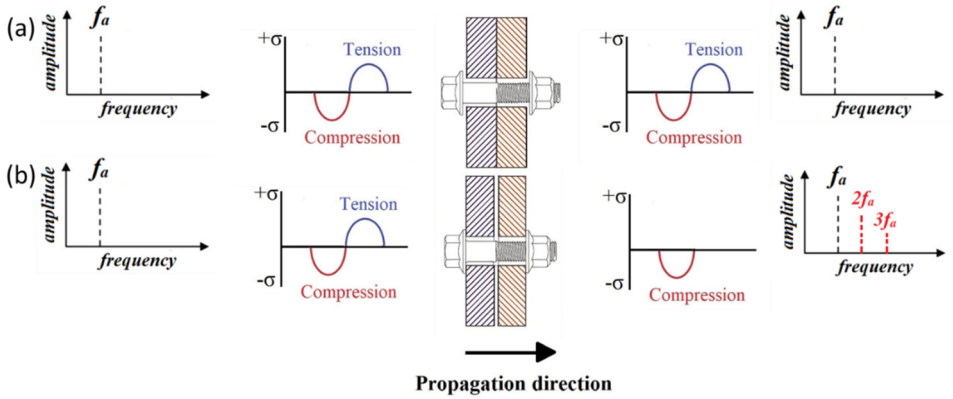

Fig. 1 Schematic diagram of CAN generation at: (a) a tight bolt; and (b) a loose bolt

predict because its scattering direction is independent of the incident wave's propagation direction.

1.3 Guided waves applications for detecting imperfect bolted joints

In the literature, the number of researches on the application of guided waves for the non-destructive evaluation of bolted joints is limited to a few studies.

Wang *et al*. (2013) studied the effect of bolted joint's preload on the incident wave energy. It was shown that the applied torque is proportional to the wave energy scattered from the bolted joint. In addition, a time-reversal scheme was developed for the non-destructive evaluation of bolted joints (Wang *et al*. 2016). However, as it has been already discussed, there are some limitations in using linear guided waves for damage detection. The need for baseline data and multiple boundary reflections in the small or complex structure are some of the linear guided waves' drawbacks (An and Sohn 2010). Unlike linear wave parameters, the nonlinear wave parameters have shown a better potential for the structural health monitoring of complex structures or the ones that serve under varying and harsh conditions. The generation of higher harmonics by CAN is one of the favorable nonlinear features of guided waves for nondestructive evaluation. The CAN is generated because of repetitive clapping of the breathing damage's surfaces when the guided wave collides with the damage.

During the collision, the wave becomes distorted because the compressive part of the wave can penetrate through the closed surfaces whereas the tensile part cannot. The wavelength is modified because of the distortion caused by the defect's surfaces leading to the CAN and Higher Harmonics Generation (HHG). Therefore, the response of the system contains additional frequency components. Figs. 1(a) and 1(b) show the schematic diagram of the interaction of a sinusoidal wave packet with a fully tight and a loose bolted joint respectively. As can be seen from these figures, the response of the fully tight bolt only contains the incident wave frequency whereas the response of the loose bolt contains higher harmonics of the incident wave indicating imperfect joints.

Biwa *et al*. (2006) studied and formulated the propagation of the longitudinal waves through a contact interface pair in a 1D medium. Linear and nonlinear deformations are caused by the normal force or pressure exerted on the contact surface expressed as

$$P(h) = P_0 - K_1 \times (h - h_0) + K_2 \times (h - h_0)^2 \quad (1)$$

where P is the applied pressure, h is the contact pairs gap opening, h_0 is the contact pair initial gap, P_0 is the static applied pressure, K_1 is the linear, and K_2 is the nonlinear stiffness factors. The following equation provides an approximate solution of the scattered wave as a displacement for a harmonic wave

$$D_T(t) = \frac{K_2 A_0^2}{K_1\left[1+\frac{4K_1^2}{(\rho\omega v)^2}\right]} + \frac{2K_1 A_0}{\rho\omega v\sqrt{1+\frac{4K_1^2}{(\rho\omega v)^2}}}\cos(\omega t - \delta_1) - \frac{K_2 A_0^2}{\rho\omega v\left[1+\frac{4K_1^2}{(\rho\omega v)^2}\right]\sqrt{1+\frac{4K_1^2}{(\rho\omega v)^2}}}\sin(2\omega t - 2\delta_1 + \delta_2) \tag{2}$$

where ω is the incident angular wave frequency, A_0 is incident wave amplitude, ρ is the material density, v is the longitudinal wave velocity, $\delta_1 = tan^{-1}\left(\frac{\rho v\omega}{2K_1}\right)$ and $\delta_2 = tan^{-1}\left(\frac{K_1}{\rho v\omega}\right)$. As is obvious in Eq. (2), in the third term, there is the higher harmonics component whose angular frequency is double that of the incident wave frequency. Lee and Jhang (2009), used nonlinear bulk waves for detecting the fatigue cracks in the aluminum blocks. Their results indicate that the magnitude of applied pressure on the cracked surface inversely affects the second harmonic of the bulk wave's magnitude. Biwa *et al*. (2006) studied the influence of applied pressure on the contact area between two aluminum blocks. The results show that the bulk wave's second harmonic magnitude inversely changes with applied contact pressure and the applied contact force. These are a few examples of the successful application of bulk waves for the nondestructive evaluation of bolted joints. However, the studies also indicate that the bulk waves-based nondestructive evaluation is suitable for the localized evaluation of the structures. However, in most situations, the bulk waves-based evaluation may not be suitable when the inspection area is inaccessible.

Unlike bulk waves, the guided waves inspection technique can inspect a large area and can cover inaccessible parts. Therefore, in recent years, several studies worked on the application of nonlinear guided waves for the nondestructive evaluation of bolted joints (Amerini and Meo 2011, Zhang *et al*. 2017a, b). Amerini and Meo (2011) used nonlinear guided waves for the nondestructive evaluation of bolted joints. It was shown that when a bolt is loosened, the spectral amplitude difference between the incident and the second harmonic frequencies is smaller than when it is tightened. In this study, a function was developed to predict the amplitudes of the spectral components corresponding to different magnitudes of applied torque. Zhang *et al*. (2017a) proposed a sub-harmonic resonance-based technique for detecting loosened bolts using guided waves. Zhang *et al*. (2017b) developed a vibro-acoustic modulation approach and proposed a sideband frequency index for the nondestructive evaluation of composite and metallic bolted joints. Zhao *et al*. (2020) developed a real-time nonlinear ultrasonic method using vibro-acoustic modulation for the early detection of loose bolts using piezoelectric transducers. In their study, they managed to deliver a low-cost vibro-modulation method using a lead zirconate titanate patch which is able to successfully detect the loose bolts.

As discussed, there has been a succession of works focused on using the nonlinear guided waves technique for detecting imperfect bolted joints. However, most studies are focused on bolt loosening detection and there have been limited studies conducted on locating the loosened bolts.

This could be an issue when the inspection area consists of multiple bolted joints because the location of the loose bolt still needs to be found for repair/maintenance purposes. However, this study uses an efficient signal processing approach to deliver an all-in-one seamless method for detecting and locating loose bolts using the data obtained from damage detection without a need for conducting further tests or using additional equipment for damage localization. Hence, compared to other discussed methods which can detect the loose bolts only, the proposed method could be more efficient and faster for bolted joints' maintenance and monitoring.

1.4 Article objectives

This research is different from the previous studies because it aims at addressing some of the existing gaps in the application of nonlinear guided waves. This study is conducted in two main phases. In the first phase, the study investigates the possibility of using CAN and the HHG for detecting loose bolts in bolted joints. The second phase processes and uses the data obtained from phase 1 for developing a seamless approach for locating the loose bolts.

This study is a comprehensive numerical and experimental study and may provide further physical insights into understanding the CAN generation and HHG in loose bolts. The study outcomes may enhance the nondestructive evaluation and maintenance of the bolted joints using nonlinear guided waves. A wide range of industrial sectors such as aviation, construction, oil and gas, and car manufacturing may benefit from the outcomes of this research.

This article is organized in the following order: Section 0 discusses the damage detection and damage localization methodologies used in this study. Section 4 is focused on discussing the experimental setup and results for detecting and locating loose bolts in bolted joints. In Section 0, a 3D FE simulation approach is developed for predicting the propagation of guided waves in loose bolts which is verified using experimentally acquired data. A set of damage cases are created and studied in this section as well. Section 5 presents the study conclusions.

2. Damage detection and localization methodology

2.1 Damage detection

In common practice, most common guided wave techniques use baseline data for nondestructive evaluation and assessment. However, this study aims at delivering a baseline-free approach by utilizing nonlinear features of guided waves such as HHG to detect and locate the loose bolts. Therefore, the proposed approach is advantageous over other common nondestructive testing techniques because it does not require the baseline data.

Previous works (Soleimanpour and Ng 2017, Fromme and Sayir 2002) show that for the same excitation frequency, the asymmetric mode of guided waves (A_0) has a smaller wavelength and larger out-of-plane displacement magnitude than the symmetric mode (S_0). In addition, when the defect orientation is normal to the propagation direction, the A_0 mode provides a larger contact pressure and thus a larger higher harmonic magnitude is obtained at the loose bolt. Therefore, in this study, A_0 guided wave mode is preferred over S_0 mode and is used for detecting and locating loose bolts.

2.2 Transducers configuration

The study uses a network of sensors consisting of two piezoelectric transducers for damage

detection and damage localization. Generally, there are two sensor configurations depending on the position of sensors and defect referred to as pulse-echo and pitch-catch configurations. Previous works (Zhang *et al*. 2017a, b) show that although both configurations can detect and locate the defects, the pulse-echo configuration is more robust for damage localization. Therefore, in this work, the pulse-echo configuration is used. In the pulse-echo sensor configuration, both the actuator and receiver sensors are located on the same side of the damage. Therefore, the receiver captures the reflected nonlinear wave packets which can be used for detecting and locating the loose bolt.

2.3 Damage localization

When pulse-echo is used, incident waves first arrive at the receiver, then at the loose bolt. The incident wave also may collide with the medium's boundaries and be reflected. The reflected wave packets from the loose bolt may mix with the reflected waves from the boundaries and arrive at the receiver later. This is not desired when the linear wave technique is used because the reflected wave packets from the defect may not be detected due to multiple captured overlapped wave packets. However, the collision of the incident wave with the loose bolt's surfaces leads to HHG and CAN generation. The nonlinear wave packets may still be mixed with linear waves and arrive together at the receiver. However, this will not influence damage detection and damage localization using nonlinear wave packets. The captured linear wave packets propagate at the incident wave (f_c) whereas the nonlinear wave packets propagate at the double incident wave frequency ($2f_c$). The time of arrival for the incident wave packet is denoted by (t_{f_c}) and can be calculated by

$$t_{f_c} = \frac{L_{AR}}{c_g(f_c)} \tag{3}$$

where L_{AR} is the distance between the sensors, $c_g(f_c)$ is the incident wave group velocity at the excitation frequency of (f_c). The time of arrival for the nonlinear guided wave packet at the double incident wave frequency ($2f_c$) is denoted by (t_{2f_c}) and can be calculated by

$$t_{2f_c} = \frac{L_{AR}}{c_g(f_c)} + \frac{L_{BR}}{c_g(f_c)} + \frac{L_{BR}}{c_g(2f_c)} \tag{4}$$

where $c_g(2f_c)$ is the nonlinear guided wave group velocity at the frequency of $2f_c$ and L_{BR} is the distance between the receiver and the loose bolt. By using Eqs. (3) and (4), the location of the loose bolt can be estimated by

$$L_{BR} = \frac{\Delta t.\, c_g(2f_c).\, c_g(f_c)}{c_g(2f_c) + c_g(f_c)} \tag{5}$$

where $\Delta t = t_{2f_c} - t_{f_c}$, Δt is the estimated difference between the time of arrival of the incident wave (t_{f_c}) and the nonlinear wave (t_{2f_c}). By estimating the Δt, the location of the loose bolt (L_{BR}) can be determined using Eq. (5). (Soleimanpour *et al*. 2017).

In the case of using the linear guided wave technique for detecting and locating the loose bolts, the reflected wave packets from the loose bolt need to be extracted using baseline. This task can be complicated for small or complex structures, as the wave packets will overlap. Therefore, the

linear wave approach may not be able to detect and locate the loose bolt. Unlike the linear wave technique, the proposed nonlinear guided waves technique in this study uses the estimated time of arrival of the linear and nonlinear guided waves packets for damage detection and damage localization which can be simply calculated using the Continuous Wavelet Transform (CWT) even if the individual signals cannot be extracted.

2.4 Signal processing

The application of signal processing using Hilbert Transform (HT), Fast Fourier Transform (FFT), Inverse Fast Fourier Transform (IFFT), and the CWT can ehance the nondestructive evaluation of the structures (Yu and Giurgiutiu 2005, Ng 2014). As discussed in Section 2.3, the current study uses the time of arrival to conduct damage detection and damage localization. Therefore, the signal processing in the current study aims at estimating the required parameters using a combination of HT, FFT, IFFT, and CWT. In this section, the signal processing scheme used in the current study is discussed in detail.

The experimental and numerical data is initially acquired in the time domain. The signal envelope is calculated by HT and is used for calculating the time of arrival for the incident wave packet (t_{f_c}). The time-domain data is processed using FFT to transform the data from the time domain to the frequency domain to determine the available frequency components in the captured signals. The existence of frequency components different from the incident wave frequency indicates an imperfect bolted joint. A high pass filter is used to filter the data and eliminate unwanted frequency components. In this study, the Butterworth filter is used for processing the data. The filtered data is processed in the time-frequency domain using CWT which can also enhance the observation and estimation of the time of arrival of different wave packets at their corresponding frequencies.

The CWT displays the scale-dependent structure of a signal such as frequency against time. Hence, CWT shows the frequency versus time for a signal. It is possible to calculate the wavelet coefficient $WT(m,n)$ by convolving the measured guided wave signal $u(t)$ with the translation m and dilation n values as (Ng 2014)

$$WT(m,n) = \int_{-\infty}^{\infty} u(t)\chi_{m,n}^{*}(t)dt \tag{6}$$

where

$$\chi_{m,n}^{*}(t) = \frac{1}{\sqrt{n}}\,\chi\left(\frac{t-m}{n}\right) \tag{7}$$

where $\chi(t)$ is the mother wavelet. In the current study, the Gabor wavelet is used as the mother wavelet.

3. Damage detection and damage localization experiments

3.1 Experimental setup

The experimental study considered a double-lap connection consisting of two bolts. The specimen is made up of two A36 steel plates with 110 mm × 20 mm × 2.5 mm dimensions and the

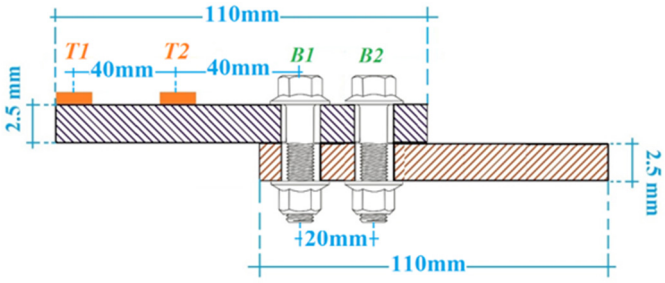

Fig. 2 Schematic diagram of specimen used in the experiment

Table 1 Mechanical properties of the A36 grade steel plate

Modulus of elasticity	200 GPa
Density	7850 kg/m^3
Poison's ratio	0.26

bolts of 11 mm diameter made from A307 grade steel located 20 mm from each other center to center. The schematic diagram of the specimen is shown in Fig. 2. The mechanical properties of A36 steel plates are presented in Table 1.

The length of the specimens is considered relatively short. Therefore, there will be several wave reflections from the boundaries which may overlap with other wave packets. Therefore, extracting the incident wave packet and the scattered wave packets from the loose bolt may not be possible. This was intentionally done to demonstrate the advantage of using nonlinear guided waves over linear guided waves technique for similar cases. Bolts were tightened using a torque wrench equipped with electronic measurements for recording the applied torque magnitudes. Two 10 mm × 5 mm × 1 mm rectangular piezoelectric transducers were adhesively bonded to the top surface of the plates (Fig. 2). The sensors were positioned in pulse-echo configuration and the excitation signal was generated using transducer 1 (*T*1) while transducer 2 (*T*2) was used as the receiver sensor. The distance between *T*1 and *T*2 was measured as 40 mm center to center.

The output voltage of the function generator was amplified from 10 volts to 80 volts peak to peak using a PD-200, 60 watt, PiezoDrive amplifier before applying it to the transducer.

The amplifier distortion rate at 140 kHz excitation frequency was calculated as 0.5%. This was calculated to ensure that there is no or very small equipment-related nonlinearity and thus the

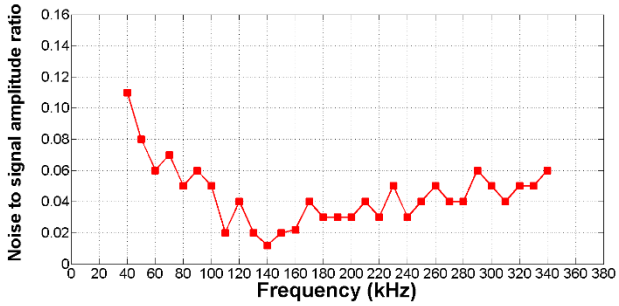

Fig. 3 Experimental noise amplitude ratio for different incident frequencies

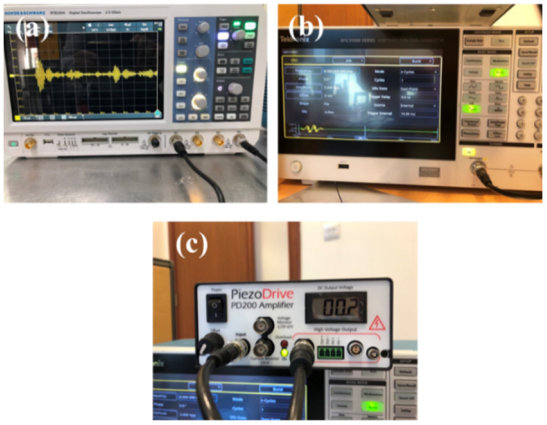

Fig. 4 Experimental equipment used in the study: (a) Signal oscilloscope; (b) arbitrary function generator; and (c) amplifier

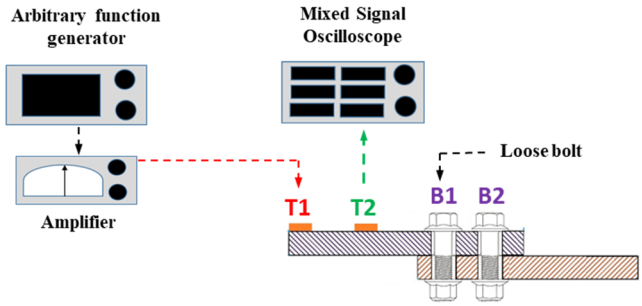

Fig. 5 The experiment setup schematic diagram

CAN is the only source of HHG in the captured signal. The output signal was captured by the receiver piezoelectric transducer which was connected to a Rohde & Schwarz RTB2K-COM4 300 MHZ, 2.5 GS/s, and 20 Mpts memory depth mixed signal oscilloscope. To improve the quality of the measurement, the output signal was averaged over 100 acquisitions. Fig. 4 shows the data acquisition system used in the experiment. A schematic diagram of the experimental setup is shown in Fig. 5.

3.2 Experimental results

The arrangement is to ensure that only one of the bolts is loosened. In this case, B2 was fully clamped while B1 was clamped by a torque level that allows separation of the plates. Therefore, for B1 a torque level that will not result in full clamping of steel plates should be selected to ensure that the surfaces are free to clap. Previous studies (Yang *et al*. 2019, Ng 2014) show that the HHG is significantly influenced by the magnitude of the applied torque. The ASTM (2003) specification covers studs and carbon steel bolts ranging from ¼ in. (6.5 mm) through 4 in. (102 mm) diameter. According to the code, the recommended torque level for a $^{7}/_{16}$ in. (11 mm) A307 steel bolt is set to 19 lb.ft (26 N.m).

The torque level applied to the bolts was swiped from 6 N.m to 30 N.m in 2 N.m steps. The

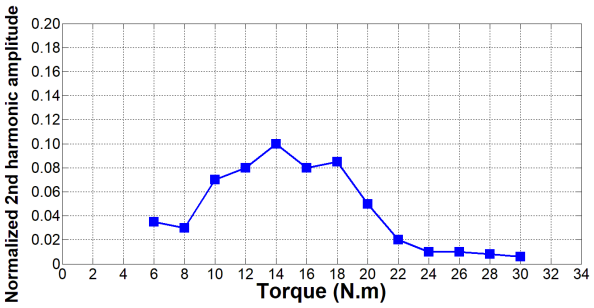

Fig. 6 Variation of measured normalized second harmonic amplitude against applied torque level

data was captured at the receiver and processed using the method discussed in Section 2.4. The results showed no or very small second harmonic amplitude when the torque level exceeds 22 N.m whereas the 14 N.m torque level provided the largest acquired second harmonic amplitude of guided waves. Therefore, B2 was tightened by 25 N.m (fully clamped) whereas the torque level for B1 was set to 14 N.m. Fig. 6 shows the variation of measured normalized second harmonic amplitude with applied torque on the bolts.

3.2.1 Damage detection

Figs. 7(a) and 7(b) show the captured data in the time domain and the frequency domain, respectively. As shown in Fig. 7(a), the data in the time domain contains several mixed wave packets, and thus, extracting the reflected wave packet from the loose bolt may not be possible. Therefore, without a baseline, the linear wave technique may not be able to detect and locate the loose bolt. Although the excitation signal is a 140 kHz five-cycle tone burst narrow band signal, the received response signal's bandwidth is wider than that of the incident wave frequency and thus contains other frequency components. As such, the HHG can be easily observed in Fig. 7(b) which confirms the existence of the loose bolt.

However, the time-frequency domain data can provide further information such as the magnitude of scattered wave packets, the time of arrival, and the corresponding frequencies for each wave packet. Fig. 7(c) shows the captured data in the time-frequency domain using CWT. The time of arrival for each wave packet at the sensor can be obtained from this figure. However, only the linear wave contours at the central frequency of 140 kHz appear in the graph because the magnitudes of the wave packets at other central frequencies are very small and thus those contours will not be visible. Therefore, the contours for linear and nonlinear wave packets do not appear simultaneously in the same CWT graph. To show the higher harmonic frequency wave packet contours in the CWT graph, we need to get rid of the linear wave packets by using a high pass filter. Therefore, a high pass filter was applied to the frequency domain data to remove the unwanted frequency components. This was followed by an IFFT to return the data to the time domain. Figs. 8(a) and 8(b) show the time-domain and CWT of the captured data after applying the filter, respectively.

Unlike the previous CWT graph (Fig. 7(c)), the energy contour for the guided waves at the second harmonic frequency can be detected in this graph which provides important information about the nonlinear wave packets. In the graph, there are multiple mixed wave packets at the second harmonic of guided waves frequency. Detecting the source of each wave packet may not be possible as they are mixed and also due to the small and complex geometry of the specimen.

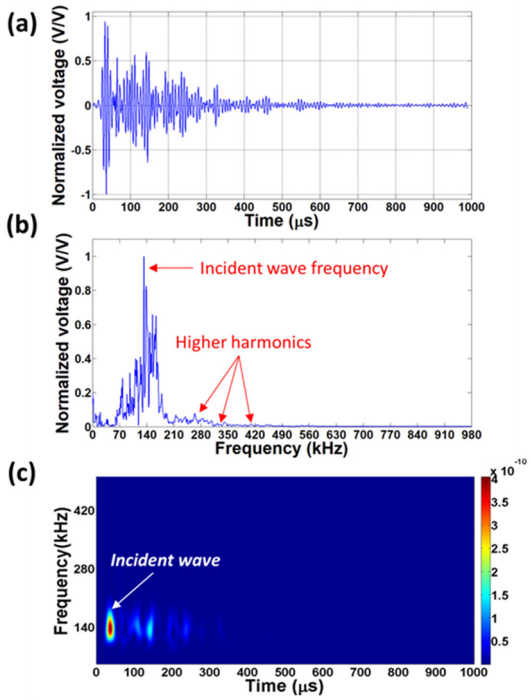

Fig. 7 Experimental data in: (a) time; (b) frequency; and (c) time-frequency domain

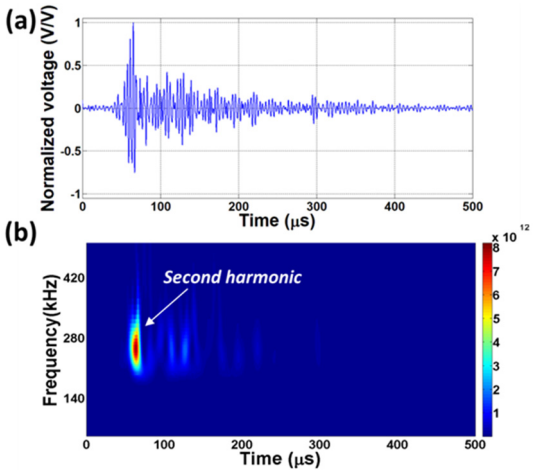

Fig. 8 Experimental filtered data in: (a) time-domain; and (b) time-frequency domain

However, these wave packets can be attributed to the interaction of linear waves reflected from the boundaries with contact surfaces or they may be generated by multiple clapping of loose bolt surfaces. These wave packets will arrive at the receiver with a smaller amplitude. The reason for the amplitude of the abovementioned wave packets being small is due to the smaller linear wave packet amplitude that generates those nonlinear wave packets and also due to the wave attenuation by the material damping. However, the results indicate that the nonlinear wave packet with the

largest amplitude is generated immediately after the initial arrival and interaction of the incident wave with surfaces of loose bolted joints. This can be confirmed using the time of arrival and the group velocity of the second harmonic frequency wave packet and the propagation distance which is discussed further in Section 3.2.2.

3.2.2 Damage localization

In the previous section, the experimental observations confirmed the existence of the breathing defect in the bolted joint. However, to locate the damage, the time of arrival for the linear and nonlinear wave packets needs to be determined. As discussed in Section 2.4, the time of arrival for linear and nonlinear guided wave packets is estimated using the signal envelope.

Therefore, the signal envelope was calculated for both unfiltered and filtered data. The arrival time for linear wave (t_{f_c}) and the second harmonic frequency (t_{2f_c}) was estimated as 36.6 µs and 66.6 µs, respectively yielding a time difference (Δt) of 30 µs between the time of arrival of linear and nonlinear wave packets. The group velocities for 140 kHz and 280 kHz asymmetric guided waves $c_g(f_c)$ and $c_g(2f_c)$ were calculated as 2708 m/s and 3100 m/s using DISPERSE (Lowe & Pavlakovic. 2013), respectively. The estimated time of arrival for the incident wave at T2 using the group velocity of linear guided waves over a propagation distance of 40 mm is 32.7 µs which matches the time of arrival for the first contour in Fig. 7(c). This confirms that the first contour is the energy contour for the incident wave which arrives first at T2. Also, the estimated time of

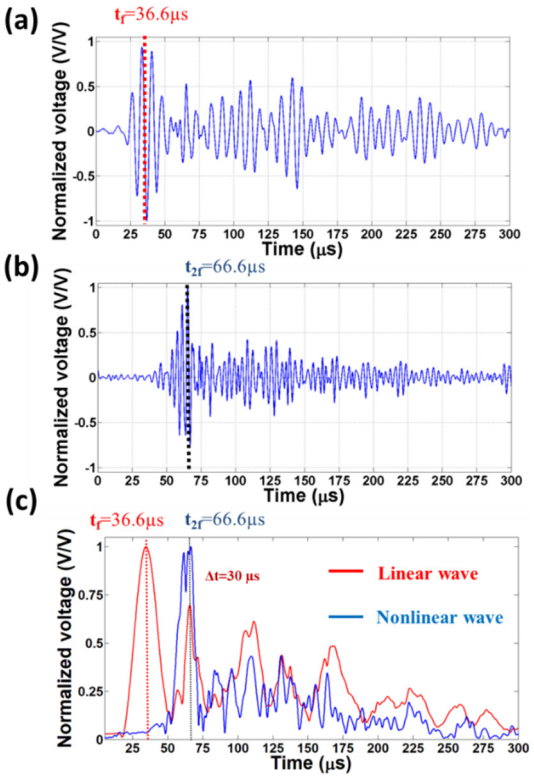

Fig. 9 Time domain data for: (a) unfiltered data; (b) filtered data; and (c) signal envelope for the linear and nonlinear wave packets

arrival for the reflected nonlinear wave packet from loose bolt using group velocity of linear and nonlinear guided waves over a propagation distance of 120 mm is 60.3 μs which matches the time of arrival for the first contour in Fig. 8(b). Therefore, the first contour with the largest energy in Fig. (b) is the energy contour for the nonlinear wave reflected from the loose bolt which arrives at T2 following the arrival of the incident wave which is in good agreement with the real distance (40 mm center-to-center). Using Eq. (5), the distance between T2 and B1 (L_{BR}) is calculated as 43.4 mm. Although the center of the loose bolt to T2 is 40 mm, the bolt surfaces which are the source of CAN are located within $L_{BR} \pm D/2$ from T2 (is the nominal bolt diameter). Hence, the true loose bolt location falls within 34.5 mm to 45.5 mm from T2. As can be seen, the estimated location (43.5 mm) is within the range of the true loosened bolt surface. Therefore, the location of the loosened bolt was estimated successfully. The normalized signal envelope for both data sets is shown in Fig. 9(c) which shows the time of arrival for the linear and nonlinear wave packets. Multiple hikes in the filtered signal envelope (red curve) indicates further generated nonlinear wave packets discussed in Section 3.2.1.

4. 3D FE simulation

4.1 Modeling methodology

ABAQUS was used to model the experimental setup using 3D explicit FE simulation. Eq. (7) was recommended by Caccese *et al*. (2004) for the calculation of the bolt tightening pressure which was used in the FE models.

$$P = \frac{T}{kDA} \tag{8}$$

In this equation, P is the estimated bolt tightening pressure, T is the applied tightening torque on the bolt, k = 0.2 is the torque coefficient, A is the washer area, and D is the nominal bolt diameter. In the 3D FE models, for simplicity, the pressure area was assumed to be a rectangular area with a width that was equal to the plate's width and a length that was twice the bolt's diameter. The other details such as the bolt hole size, the plate size, and the material properties in the 3D FE models were identical to those used in the experimental study. Eight-noded linear brick full integration elements referred to as C3D8 elements were used for modeling the specimens. The hourglass energy was restricted to less than 1.5% of the overall energy to maintain the stability of the simulation. A 0.2 mm × 0.2 mm × 0.2 mm mesh size was used in FE models. By doing so, it is ensured that there are more than 20 elements per wavelength and 12 elements over the thickness of the steel plates, which will allow for accurate modeling of the asymmetric guided wave mode shape. The excitation signal was the same as what was used in the experiment. To generate the asymmetric guided wave in the 3D FE models, out-of-plane displacement was applied to nodes on the plate's top surface of the same area and size as the piezoelectric actuator.

The loose bolt was simulated by splitting the nodes at the loose bolt which was carried out by inserting a "Seam crack" between two plates at the loose bolt area. To prevent interpenetration of the loose bolt's surfaces and to model the clapping mechanism, a pair of native mesh surfaces was assigned to the surfaces of the loose bolt. The surface-to-surface contact interaction was also assigned to the loose bolt's surfaces to simulate the interaction between the surfaces of the loose bolt. Soleimanpour *et al*. (2017) successfully used this approach in previous studies.

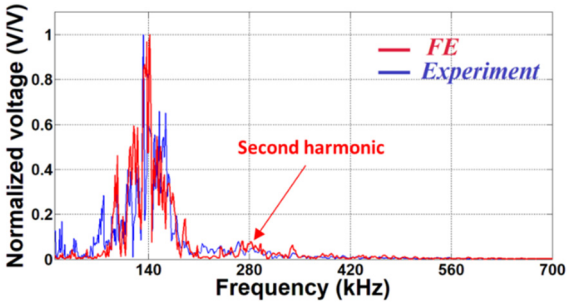

Fig. 10 Comparison between experimental & numerical data in the frequency domain

To simulate the wave attenuation, Rayleigh stiffness proportional and mass proportional damping coefficients were used to implement the material damping in the 3D FE models. Also, to simulate the noise effects, white noise was added to the time-domain response signal, which was 1.2% of the signal's maximum amplitude. This noise level was obtained from the experiment.

4.2 Validation of 3D FE model

Fig. 10 compares the experimental with the numerical results in the frequency domain. As shown, both approaches are in good agreement because HHG is available in both results. However, the two graphs do not match completely. This is because in the FE simulation, B1 was considered fully loosened while B2 was considered fully clamped and the seam crack was assigned to the full area covered by B1. However, in the real situation, although B1 is loosened, some parts may be still partially clamped and not be fully free to separate due to the applied torques. This may influence the captured higher harmonics amplitude. The method explained in Section 0 for processing the experimental data was used for processing the numerical data as well. The time of arrival for guided wave packets was calculated as 28.5 μs for the linear wave and 63.3 μs for the nonlinear waves which yield $\Delta t = 34.8$ μs. Using Eq. (4) the distance between the receiver and the loosen bolt is calculated as 50.3 mm which is close to the results obtained from the experiment (34.5 mm - 45.5 mm). However, the results from experimental and numerical approaches are not still completely identical. This issue has been discussed in Section 3.2.1. The numerical results in this section show the 3D FE simulation modeling approach used in this study can capture the nonlinear guided waves and is able to predict the propagation of guided waves in loose bolts.

4.3 Numerical case studies

To study the scattering of the guided wave in bolted joints caused by a variety of loose bolt size joints, the 3D FE model which was verified using experimental data in Section 4.2 is employed here. As mentioned, the length of the specimen used in Section 3 was considered short to show the applicability of nonlinear guided waves in complex structures for damage detection and damage localization. However, one may argue that the approach used in this study may not be applicable for detecting and locating damages in large areas. Therefore, the plate size is increased to 220 mm × 25 mm × 2.5 mm which is double the plate length used in the experimental study. However, since the length of plates' overlap at bolted joints needs to be adjusted to the nominal bolt size, the total length of the specimen varies for different case studies. Since the guided wave propagation

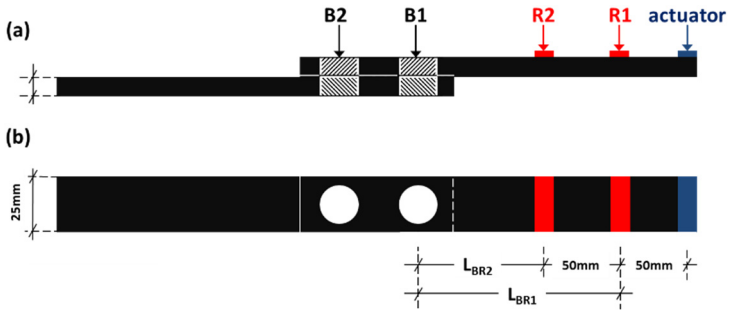

Fig. 11 Schematic diagram of 3D FE simulation model: (a) elevation; and (b) top view (1st bolt scenario)

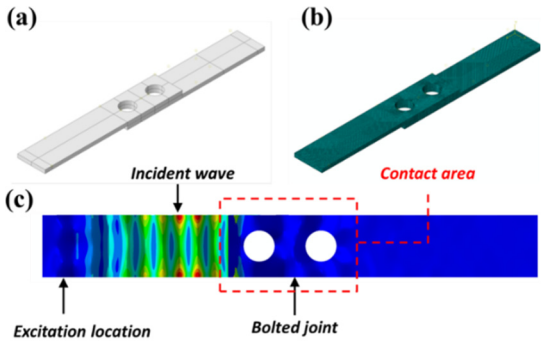

Fig. 12 3D FE model for 10 mm bolt size: (a) bolted joint model; (b) bolted joint mesh; and (c) propagation of incident wave at 50 μsec for the 1st bolt scenario

and the HHG are local phenomena, the model used in Section 3 and the long models used in this section will be different only in terms of the reflected wave packets from the boundaries. Like Section 3, there are two bolts in the bolted joint (B1 and B2). Two different bolt scenarios are considered in the numerical study. In the first bolt scenario, B1 is loosened and B2 is fully clamped whereas in the second bolt scenario the loosened and fully clamped bolts are swapped (B1 fully clamped & B2 loosened). To check the applicability of the proposed method in this study for different bolt sizes, the bolts' nominal diameter was increased in 2.5 mm increments from 5 mm to 20 mm. The schematic diagram of the 3D FE simulation modeling for the first scenario is shown in, which includes the transducer network and the locations of each transducer. As shown in Fig. 11, the network of sensors consisted of three piezoelectric transducers in pulse-echo configuration for excitation and data acquisition. The reason for using two receivers is to ensure that the reliability and accuracy of the proposed technique are not influenced by the location of the receiver. However, as explained in Section 3.2.2, the setup is able to detect and locate loose bolts with two sensors. Receiver1 (R1) and Receiver2 (R2) are located at 50 mm and 100 mm from the actuator, respectively. These sensors capture the out-of-plane displacement in the time domain which is processed further for detecting and locating the loose bolt. The excitation signal is identical to the experiment.

4.4 Results and discussion

Figs. 12(a)-(c) show the snapshot of the propagation of the asymmetric guided waves through

the loose bolt for the first bolt scenario and bolt size of 10 mm in the 3D FE model. In this model, the distance between R1 and R2 to the center of the loose bolt is 135 mm and 85 mm, respectively. As can be seen in Fig. 12, a surface-to-surface contact interaction was assigned to the surfaces of the loose bolt to simulate the CAN and the clapping mechanism between the loose bolt surfaces. This also prevents the interpenetration of the joint's surfaces. Fig. 13(a) shows the data captured by R2 in the time domain. Since the specimen is large, identifying some of the wave packets is possible by using the time of arrival for the wave packets. Based on the group velocity of the asymmetric guided wave, the propagation distance, and the calculated signal envelope using HT, the first wave pack is the incident wave, the second wave pack is the reflected wave from the bolted joint, and the third wave pack is the reflected wave from the plate end.

However, some of the wave packets are still mixed and may not be possible to be identified. This task is more complicated in complex geometries or when the inspection area is small. In Fig. 13(a), a few distorted wave packets are pointed out. As discussed in Section 0, the wave distortion could be an indication of HHG. However, this cannot be confirmed from the time-domain data because the wave distortions are small and hard to detect. Hence, the method explained in Section 0 was used to process the data in the time-frequency domain. Fig. 13(b) shows the time-frequency domain data for the wave packets at incident wave frequency without using any filters whereas Fig. 13(c) shows the time-frequency domain data for the nonlinear wave packets at double incident wave frequency after applying a high pass filter. Fig. 13(b) shows the energy contours for the wave packets at the incident wave frequency. As discussed, the first contour is the energy contour

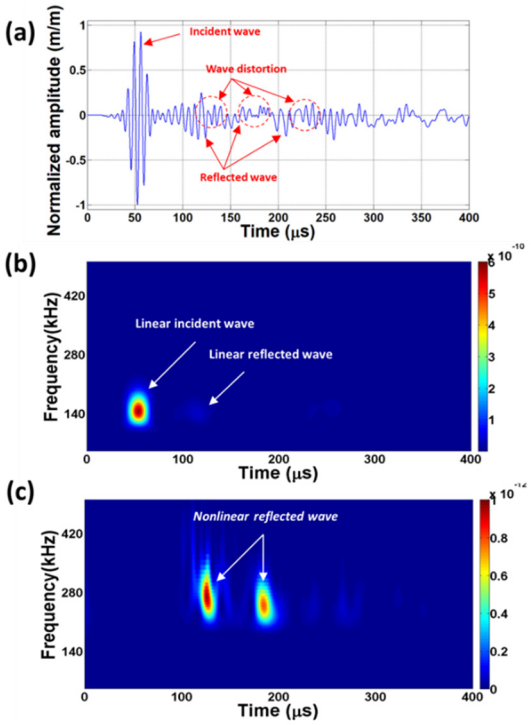

Fig. 13 Data at R2 in: (a) time-domain; (b) time-frequency domain for the incident wave frequency wave packets; and (c) time-frequency domain for the double incident wave frequency wave packets (filtered)

for the incident wave packet whereas the second weak contour is the energy contour for the wave packets that arrive later with smaller magnitudes. The nonlinear wave packets at double the incident wave frequency are visible in CWT of the filtered data presented in Fig. 13(c).

As can be seen, after processing the data using a high pass filter, several energy contours with different magnitudes have appeared in Fig. 13(c). However, these energy contours are not available in CWT of unfiltered data presented in Fig. 13(b) because of their small energy magnitudes. These two graphs are used for determining the time of arrival for the wave packets to estimate the location of the loose bolt.

As shown in Fig. 13(c), following the incident wave arrival at the receiver, several wave packets at double the incident wave frequency arrive at the sensor. The initial contour with the greatest energy is the nonlinear wave packet generated when the incident wave first collides with the loose bolt whereas the other smaller energy contours are the nonlinear wave packets generated when the boundary reflections propagate through the loose bolt or due to further clapping of loose bolt's surfaces. Again, this can be confirmed using the approach explained in Section 3.2.2.

As can be seen in Figs. 13(a)-(c), the times of arrival for the second energy contour in Fig. 13(b) and the first contour in Fig. 13(c) are identical to the time of arrival for the first reflected wave packet from the loose bolt indicated in Fig. 13(a). This means that both linear and nonlinear reflected wave packets from the loose bolt are mixed and captured by the receiver simultaneously. This justifies the wave distortions indicated in Fig. 13(a) and discussed in previous paragraphs. However, since the two wave packets propagate at different group velocities, they will separate from each other as they propagate further.

Fig. 14 shows the normalized HT for the linear and nonlinear wave packets calculated using the method discussed in Section 2.4. The times of arrival for both wave packets were calculated using this graph and are indicated by dotted lines in Fig. 14 as 53.8 µs (t_{f_c}) and 119.5 µs (t_{2f_c}) for the linear and nonlinear wave packets respectively. The difference between the time of arrival of the two wave packets (Δt) is estimated as 65.7 µs. By substituting Δt into Eq. (5) and using the group velocity of the guided waves estimated in Section 0, the location of the loose bolt (L_{BR}) is estimated as 95 mm which is very close to the true location range of the bolt surfaces from R2 (80 mm – 90 mm). Although the estimated location is very close to the true surface location, it still does not fall within the true range of the contact surface. This was investigated further and it was found that the amplitude of the higher harmonic wave packet was small due to the small bolt size which affected the accuracy of the estimated location. However, a larger amplitude of higher harmonic wave packets was acquired for larger bolt sizes.

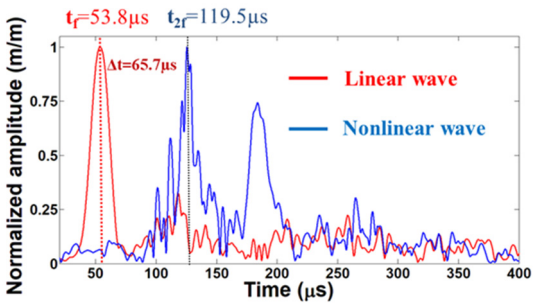

Fig. 14 Signal envelope for linear and nonlinear guided waves

The location of the loose bolt was calculated for other case studies using a similar approach. The results for different damage cases of the first bolt scenario are presented in Tables 2 and 3. Table 2 shows the estimated location (L_{BR}) versus true range of loose bolt surfaces (L_{BS}) calculated using data captured at R1 while Table 3 shows the same results obtained at R2.

Table 2 Estimated loose bolt location using captured data at R1 (1st bolt scenario)

Bolt size (mm)	Estimated time of arrival		Estimated location	True distance to the center of the bolt	True range of loose bolt surfaces
	t_{2f_c}(µsec)	t_{f_c}(µsec)	$L_{(BR)1}$ (mm)	L_B (mm)	L_{BS} (mm)
5.0	125.9	34.5	132	143	141-146
7.5	140.8	36.3	151	139	135-143
10.0	123.9	35.3	131	135	130-140
12.5	130.5	35.1	136	131	125-137
15.0	130.0	35.2	135	128	121-136
17.5	115.2	35.6	115	124	115-133
20.0	111.4	36.0	111	120	110-130

Table 3 Estimated loose bolt location using captured data at R2 (1st bolt scenario)

Bolt size (mm)	Estimated time of arrival		Estimated location	True distance to the center of the bolt	True range of loose bolt surfaces
	t_{2f_c}(µsec)	t_{f_c}(µsec)	$L_{(BR)2}$ (mm)	L_B (mm)	L_{BS} (mm)
5.0	114.6	53.0	89	93	91-96
7.5	113.6	54.8	85	89	85-93
10.0	119.5	53.8	90	85	80-90
12.5	113.0	53.5	86	81	75-87
15.0	102.8	53.7	71	78	71-86
17.5	111.5	54.1	83	74	65-83
20.0	99.4	54.4	65	70	60-80

Table 4 Estimated loose bolt location using captured data at R1 (2nd bolt scenario)

Bolt size (mm)	Estimated time of arrival		Estimated location	True distance to the center of the bolt	True range of loose bolt surfaces
	t_{2f_c}(µsec)	t_{f_c}(µsec)	$L_{(BR)1}$ (mm)	L_B (mm)	L_{BS} (mm)
5.0	136.6	53.5	120	118	116-121
7.5	134.2	54.6	115	114	110-118
10.0	132.4	54.2	113	110	105-115
12.5	128.4	53.0	109	106	100-112
15.0	130.2	53.4	111	103	96-111
17.5	125.3	54.1	103	99	90-108
20.0	125.1	53.2	104	95	85-105

Table 5 Estimated loose bolt location using captured data at R2 (2nd bolt scenario)

Bolt size (mm)	Estimated time of arrival		Estimated location	True distance to the center of the bolt	True range of loose bolt surfaces
	t_{2f_c} (µsec)	t_{f_c} (µsec)	$L_{(BR)1}$ (mm)	L_B (mm)	L_{BS} (mm)
5.0	152.0	35.1	169	168	166-171
7.5	150.3	36.1	165	164	160-168
10.0	149.9	35.8	165	160	155-165
12.5	144.5	34.5	159	156	150-162
15.0	149.0	34.9	165	153	146-161
17.5	142.8	35.6	155	149	140-158
20.0	132.0	34.7	141	145	135-155

In order to investigate the applicability of the proposed method for the second bolt scenario where B1 fully is clamped and B2 loosened, a new set of 3F FE models were created. The 3D FE models are identical to the previous models, except for the loosened and fully clamped bolt. The repeated for the second bolt scenario. Tables 4 and 5 present the loose bolt localization results for different damage cases of the second bolt scenario using data captured at R1 and R2 respectively. As shown in Tables 2 to 5, the estimated location of the loose bolt is in good match with the true range of loose bolt surfaces (L_{BS}) for all case studies and both bolt scenarios with some exceptions for bolt sizes smaller than 10 mm. Therefore, the technique provides better results for the bolt size above 10 mm. Although the results for bolt sizes smaller than 10 mm do not fall within the true range, the results are still very close to the true locations. This could be because of small generated higher harmonics due to the smaller contact area of small bolt sizes. Therefore, the results show that the proposed approach in the current study can be successfully used for detecting and locating loose bolts.

5. Conclusions

This study proposed a baseline-free approach for detecting and locating loose bolts using HHG. The study used numerical and experimental approaches to develop and validate the scheme. A 3D FE simulation approach was developed for predicting the propagation of asymmetric guided waves in loose bolted joints which was validated using experimentally obtained data. To ensure the applicability of the proposed approach, a set of 3D FE models with different bolt sizes were created and studied.

The proposed damage detection and damage localization scheme in this study works with a transducer network of two transducers in the pulse-echo configuration. A multi-stage signal processing scheme using HT, FFT, IFFT, and CWT was developed for processing the output signals. The experimental and numerical results showed that the CAN causes wave distortions which can be observed in the time domain data. However, the study showed that in complex structures or small inspection areas, the time domain data may not be able to provide enough information about the existence and location of the loose bolts due to the complexity of the output data.

A high pass filter was used to extract the nonlinear guided wave packets by eliminating the

unwanted frequency components. The time of arrival for guided wave packets was calculated using the signal envelope which was used for estimating the location of the loose bolt. The estimated location of the loose bolt was in good match with the true location of the loose bolt for numerical and experimental case studies.

In summary, the results of this research show that the proposed damage detection and damage localization method can accurately detect and locate the loose bolts without the need for baseline data.

This research focused on 2D double bolted joints consisting of a single loose bolt. However, in practical conditions, the bolted joins usually consist of several bolts. Therefore, it is planned to develop this investigation further to a full-scale structural bolted joint with several bolts. This will further support the applicability of the nonlinear guided waves' features for the nondestructive evaluation of loose bolts.

Funding

This project was partially funded by the Australian University and Kuwait Foundation for the Advancement of Sciences (KFAS), under project codes RC 2018-19-SOE-CE-PR04, PR19-15EC-09, and CR20-13EV-01.

References

Amerini, F. and Meo, M. (2011), "Structural health monitoring of bolted joints using linear and nonlinear acoustic/ultrasound methods", *J. Struct. Health Monitor.*, **10**, 659-672. https://doi.org/10.1177/1475921710395810

An, Y.K. and Sohn, H. (2010), "Instantaneous crack detection under varying temperature and static loading conditions", *J. Struct. Health Monitor.*, **25**(7), 730-741. https://doi.org/10.1002/stc.394

ASTM Standard A307-07 (2017), Standard specification for carbon steel bolts, studs, and threaded rod 60,000 psi tensile strength, American Society for Testing and Materials, West Conshohocken, PA, USA. https://doi.org/10.1520/A0307-07

Biwa, S., Hiraiwa, S. and Matsumoto, E. (2006), "Experimental and theoretical study of harmonic generation at contacting interface", *Ultrasonics*, **44**, e1319-e1322. https://doi.org/10.1016/j.ultras.2006.05.010

Caccese, V., Mewer, R. and Vel, S.S. (2004), "Detection of bolt load loss in hybrid composite/metal bolted connections", *Eng. Struct.*, **26**, 895-906. https://doi.org/10.1016/j.engstruct.2004.02.008

Fromme, P. and Sayir, M.B. (2002), "Detection of cracks at rivet holes using guided wave", *J. Ultrasonics*, **40**(1-8), 199-203. https://doi.org/10.1016/S0041-624X(02)00137-3

Kumar, A., Torbert, C.J., Jones, J.W. and Pollock, T.M. (2009), "Nonlinear ultrasonics for in situ damage detection during high frequency fatigue", *J. Appl. Phys.*, **106**, 1-9. https://doi.org/ 10.1063/1.3169520

Lee, T.H. and Jhang, K.Y. (2009), "Experimental investigation of nonlinear acoustic effect at crack", *NDT & E Int.*, **42**, 757-764. https://doi.org/10.7779/JKSNT.2012.32.4.355

Lowe, M. and Pavlakovic, B. (2013), DISPERSE User's Manual Version 2.0.20a; Non-Destructive Testing Laboratory, Imperial College London, UK.

Ng, C.-T. (2014), "On the selection of advanced signal processing techniques for guided wave damage identification using a statistical approach", *Eng. Struct.*, **67**, 50-60. https://doi.org/10.1016/j.engstruct.2014.02.019

Pruell, C., Kim, J-Y., Qu, J. and Jacobs, LJ. (2007), "Evaluation of plasticity driven material damage using lamb waves", *J. Appl. Phys. Lett.*, **91**, 231911. https://doi.org/10.3390/app10155124

Richardson, J.M. (1979), "Harmonic generation at an unbonded interface—I. Planar interface between semi-infinite elastic media", *Int. J. Eng. Sci.*, **17**, 73-85. https://doi.org/10.1016/0020-7225(79)90008-9

Soleimanpour, R. and Ng, C.T. (2017), "Locating delaminations in laminated composite beams using nonlinear guided waves", *Eng. Struct.*, **131**, 207-219. https://doi.org/10.1016/j.engstruct.2016.11.010

Soleimanpour, R. and Ng, C.-T. (2021), "Scattering analysis of nonlinear Lamb waves at delaminations in composite laminates", *J. Vib. Control*, **28**(11-12), 1311-1323. https://doi.org/10.1177/1077546321990145

Soleimanpour, R. and Soleimani, S.M. (2022), "Scattering analysis of linear and nonlinear symmetric Lamb wave at cracks in plates", *Nondestr. Test. Eval.*, **37**(4), 439-463. https://doi.org/10.1080/10589759.2022.2030330

Soleimanpour, R., Ng, C.-T. and Wang, C.H. (2017), "Higher harmonic generation of guided waves at delaminations in laminated composite beams", *Struct. Health Monitor.*, **16**, 400-417. https://doi.org/10.1177/1475921716673021

Solodov, I.Y., Krohn, N. and Busse, G. (2002), "CAN: an example of nonclassical acoustic nonlinearity in solids", *Ultrasonics*, **40**, 621-625. https://doi.org/10.1016/s0041-624x(02)00186-5

Wang, F. and Song, G. (2020), "Monitoring of multi-bolt connection looseness using a novel vibro-acoustic method", *Nonlinear Dyn.*, **100**, 243-254. https://doi.org/10.1007/s11071-020-05508-7

Wang, Y., Zhu, X., Hao, H. and Ou, J. (2009), "Guided wave propagation and spectral element method for debonding damage assessment in RC structures", *J. Sound Vib.*, **324**, 751-772. https://doi.org/10.1016/j.jsv.2009.02.028

Wang, T., Song, G. and Wang, Z. (2013), "Proof-of-concept study of monitoring bolt connection status using a piezoelectric based active sensing method", *Smart Mater. Struct.*, **22**, 087001. https://doi.org/10.1088/0964-1726/22/8/087001

Wang, T., Liu, S. and Shao, J. (2016), "Health monitoring of bolted joints using the time reversal method and piezoelectric transducers", *Smart Mater. Struct.*, **25**, 025010. https://doi.org/10.1088/0964-1726/25/2/025010

Wang, F., Ho, S.C.M. and Song, G. (2019), "Modeling and analysis of an impact-acoustic method for bolt looseness identification", *Mech. Syst. Signal Process.*, **133**, 106249. https://doi.org/10.1016/j.ymssp.2019.106249

Yang, Y., Ng, C-T. and Kotousov, A. (2019), "Bolted joint integrity monitoring with second harmonic generated by guided waves", *Struct. Health Monitor.*, **18**(1), 193-204. https://doi.org/10.1177/1475921718814399

Yelve, N.P., Mitra, M. and Mujumdar, P.M. (2017), "Detection of delamination in composite laminates using Lamb wave based nonlinear method", *Compos. Struct.*, **159**, 257-266. https://doi.org/10.1016/j.compstruct.2016.09.073

Yu, L. and Giurgiutiu, V. (2005), "Advanced signal processing for enhanced damage detection with piezoelectric wafer active sensors", *Smart Struct. Syst., Int. J.*, **1**(2), 185-215. https://doi.org/10.12989/sss.2005.1.2.185

Zhang, Z., Liu, M., Su, Z. and Xiao, Y. (2016), "Quantitative evaluation of residual torque of a loose bolt based on wave energy dissipation and vibro-acoustic modulation, A comparative study", *J. Sound Vibr.*, **383**, 156-170. https://doi.org/10.1016/j.jsv.2016.07.001

Zhang, M., Shen, Y., Xiao, L. and Qu, W. (2017a), "Application of subharmonic resonance for the detection of bolted joint looseness", *J. Nonlinear Dyn.*, **88**, 1643-1653. https://doi.org/doi.org/10.1007/s11071-017-3336-1

Zhang, Z., Xu, H., Liao, Y., Su, Z. and Xiao, Y. (2017b), "Vibro-acoustic modulation (VAM)-inspired structural integrity monitoring and its applications to bolted composite joints", *Compos. Struct.*, **176**, 505-515. https://doi.org/10.1016/j.compstruct.2017.05.043

Zhao, N., Huo, L. and Song, G. (2020), "A nonlinear ultrasonic method for real-time bolt looseness monitoring using pzt transducer–enabled vibro-acoustic modulation", *J. Intell. Mater. Syst. Struct.*, **31**(3), 364-376. https://doi.org/10.1177/1045389X19891534

CC